INVISCID/VISCOUS COUPLING INCLUDING SHOCK INDUCED SEPARATION IN TRANSONIC FLOW

H. Joona and L. Fuchs
Department of Mechanics / Applied CFD
Royal Institute of Technology
S-100 44 Stockholm, Sweden

Abstract

A direct iteration method for interactive Euler-boundary layer calculations is presented. The inviscid code is a 3D compressible Euler solver based on the Finite Volume method, with multi stage Runge-Kutta time stepping and with standard adaptive dissipation of Jameson type. Multi-Grid and enthalpy damping are used to speed up convergence. The viscous code is a 3D bondary layer code named SOBOL, which solves the first and/or second order boundary layer equations. The coupling between these two codes is made with transpiration boundary conditions. The method is natural and efficient for attached flows. If shocks are present, strong enough to cause separation, the method fails since the boundary layer equations are no longer valid. To deal with this problem a defect correction technique is implemented into the coupled solver. In regions of separated flow, the effective marching direction in the boundary layer equations is always in the local flow direction. The solution is driven towards the Navier-Stokes solution iteratively. The method can cope with reattached flows, ie separation bubbles. Numerical results for shock induced boundary layer separation in transonic flows past wings are presented. The test case geometries are the RAE 2822 and the NACA 0012 airfoils for 2D flows, and the DLR F5 wing for 3D flows.

Introduction

During the past few years there has been a lot of progress in the development of numerical procedures for solving the flow field around aerodynamic configurations. A major drawback with such solvers is that they require large amounts of computational time and storage. To use a Reynolds averaged Navier-Stokes solver in an aerodynamic design process is very expensive, even with modern super-computers. The main reasons for this are that the viscous regions require a large amount of grid points and the slow convergence of the solvers. However, the viscous effects are in many flow problems restricted to small regions close to solid walls, ie in boundary layers. For attached or weakly separated flows, the high costs can be reduced with a coupled Euler-Boundary layer approach. The computational effort saved with such an approach is considerable. The Euler code can use a much coarser grid than the Navier-Stokes solver and the boundary layer is solved in a single downstream march, since the equations in the non-separated boundary layer are parabolic. Moreover, higher numerical resolution can be more easily achieved in the viscous regions with a boundary layer solver than with a Navier-Stokes solver. Inviscid/viscous coupling methods are very accurate in flows without separation. If strong enough shocks are present, separation may occur, and the coupling method fails since the boundary layer equations are no longer valid, and they cannot be integrated in the "wrong" direction.

The objective here is to develop a direct iterative method for interactive Euler-Boundary layer calculations, with emphasis on three-dimensional transonic wing calculations. Transpiration boundary conditions are used together with zero normal gradients of velocity and enthalpy in the coupling process at non-separated or mildly separated regions. A defect correction technique is introduced to boost the calculations towards the Navier-Stokes solution in separated regions. For large separation regions the inviscid and viscous solutions are matched at the boundary layer outer edge. The airfoils RAE 2822 and NACA 0012 are used as two-dimensional test cases, and in three dimensions the flow past the DLR F5 wing is computed.

The Computer Codes

The Euler solver developed here is based on Jameson's [5] method, extended to 3D Multi-Block configurations. A cell centered Finite Volume space discretization is applied, yielding second order accuracy in space if the mesh is sufficiently smooth. The time marching procedure is utilizing an explicit four stage Runge-Kutta time stepping scheme with local time steps. To capture discontinuities, like shock waves, a second order artificial viscosity term is added. Also a fourth order artificial dissipation term must be added to avoid

odd/even oscillations. The Multi-Grid method is used together with enthalpy damping to speed up the convergence. The MG-cycle used here is the sawtooth cycle.

The viscous code is a 3D boundary layer solver (SOBOL). It is used for laminar and turbulent compressible flows including the effects of surface curvature and external flow gradients. The turbulence model used in the present work (within SOBOL) is the Cebeci-Smith model. The discrete boundary layer equations are solved with a space marching finite difference method of second order. SOBOL was originally developed by Prof. F. Monnoyer. A more detailed description of the second order boundary layer theory and the numerical aspects of SOBOL can be found in [9] and [10].

Inviscid/Viscous Interaction

The interactions between the inviscid and viscous parts of the flow can be divided into weak and strong interaction regions. Weak interaction occurs for attached boundary layers and strong interaction occurs in those parts of the flow where the boundary layer equations are no longer valid, ie where shocks and separation are located. The wake behind a wing is also a region with strong interaction. Generally speaking, an inviscid-viscous coupling approach should have this in mind. In weak interaction regions the Euler equations should be coupled with the boundary layer equations, but in strong interaction regions there should be an Euler/Navier-Stokes coupling. This of course puts demands on the matching of three different solvers, each on a suitable grid. The approach adopted here is to retain the Euler and the boundary layer solvers in both weak and strong interaction regions. In order to account for separated flow effects the boundary layer equations are driven in the strong interaction regions, within an iterative process, toward the Navier-Stokes solution.

The coupling procedure must also distinguish between flow cases with only weak interactions and flow cases where strong interaction occurs. For a fully attached flow case (weak interaction), the coupling procedure can be understood from the asymptotic matching theory of VanDyke [13]. Since the boundary layer code (SOBOL) solves both the first and second order equations the procedure is as follows. First, the initial fully converged Euler solution is computed in the outer inviscid region, giving the first order Euler solution. Then, the initial first order boundary layer solution is computed, where the Euler solution from the surface is used for the outer boundary condition. This gives the equivalent inviscid source distribution to be used for the second order fully converged Euler solution. Finally the second order boundary layer is computed, where the driving Euler solution is given on surface normals. If strong interaction occurs a different approach must be taken, since the first order Euler solution may contain errors, eg the shock can be located at a wrong position. The process adopted here is to iterate between inviscid and viscous calculations. A typical number of Euler time steps between every viscous evaluation is 50-100.

Euler-SOBOL Interaction

The inviscid flow field is affected by the displacement effect of the boundary layer. The displacement thickness δ^* is defined from the relation that the mass flux in the presence of the boundary layer is equal to the mass flux in an inviscid flow terminating at δ^* instead of terminating at the wall. Lighthill [8] pointed out that the boundary layer displacement effects on the inviscid flow can be modeled by a distribution of mass sources on the physical body surface. The strength of the sources is given by the displacement thickness growth as

$$(\rho u_n)_w = \frac{d}{ds}(\rho_e u_e \delta^*) \tag{1}$$

where subscripts w and e denote the wall and the boundary layer outer edge respectively, ρ is the density, u_n is the normal velocity and s is the tangential coordinate along the surface of the body. Imposing a distribution of sources on the surface produces a displacement of the inviscid streamlines which is equivalent to adding the displacement thickness to the physical body. The advantage of using equation (1) in an iterative coupling process is that the computational grid for the inviscid calculations remains unchanged as compared to the inviscid case. The sources appear as solid surface boundary conditions in the inviscid solver.

Specifying only a mass source for the Euler calculations may result in a thin vortical region near the surface. Consequently, momentum- and enthalpy sources should also be specified at the surface. Another approach (Whitfield *et al.* [14]) is to use reflection boundary conditions enforcing the normal derivatives of the velocity and enthalpy to zero at the surface, ie

$$\frac{\partial u_n}{\partial n} = \frac{\partial H}{\partial n} = 0 \tag{2}$$

The pressure is obtained by extrapolating from the inside of the computational domain. Equations (1) and (2) together with the pressure define the conditions at the surface.

The initial Euler solution does not have to be fully converged in the iterative coupling procedure described above. In order to allow for a smooth introduction of the equivalent inviscid sources a relaxation procedure is adopted. Suppose that an Euler solution

exists after iteration k, obtained with a source distribution $(\rho u_n)^k$. The following boundary layer calculation will give a new source distribution $(\rho u_n)^{k+1}$. Before starting to calculate a new Euler solution the sources are updated, using an under-relaxation factor in the range 0.5-1.

Coupling Method for Separated Flows

In the case of separated flows the coupling process described above will be impossible since the underlying assumptions behind the boundary layer approximation are invalid. Furthermore, the boundary layer marching methodology is unstable. This implies that the equivalent source distribution in the separated regions cannot be computed. In SOBOL, the sources are extrapolated to such separated regions. Thus, the boundary layer solver has to be modified to cope with the stability and with the accuracy problems. The first difficulty is remedied by using locally an "upwind" scheme and downstream/upstream marching in the separated region. When the marching is done in the "wrong" direction, the local variable is not updated, that is the corrections at "wrongly" advanced nodes are set to zero. If one will not use locally up- and downstream marching, one may introduce an auxiliary variable $\tilde{\mathbf{q}} = (\rho, \mid v^1 \mid, \mid v^2 \mid, \mid v^3 \mid, e)$, where $\bar{\mathbf{q}} = (\rho, v^1, v^2, v^3, e)$ is the usual set of dependent variables, that is the density, velocity vector components and internal energy. For the variable $\tilde{\mathbf{q}}$ there are no stability difficulties and a downstream marching will always be done in the correct "time-like" direction. This single directional marching is equivalent to the forward/backward marching approach, and therefore we describe in more detail the uni-directional marching scheme. When using the auxiliary variable $\tilde{\mathbf{q}}$, one may describe the defect correction algorithm in the following way:

- Step 0.

  Solve the basic problem

  $$SOB(\bar{\mathbf{q}}) = 0 \tag{3}$$

  where SOB denotes the modified discretized operator in SOBOL solving the boundary layer continuity-, momentum- and energy equations. Regions where boundary layer separation is detected are marked and the following "booster" technique is applied iteratively in the regions that are extended up- and downstream of the separation bubble.

- Step 1.

  Generate the auxiliary variable $\tilde{\mathbf{q}}$.

- Step 2.

  Compute the defect $\mathbf{R}_S$ by

  $$\mathbf{R}_S^n = SOB(\tilde{\mathbf{q}}^n) - NS(\bar{\mathbf{q}}^n) \tag{4}$$

  where the superscript n denotes the iterative step. NS denotes the Navier-Stokes operator evaluated with second order central differences.

- Step 3.

  Solve, by space marching

  $$SOB(\tilde{\mathbf{q}}^{n+1}) = \mathbf{R}_S^n \tag{5}$$

- Step 4.

  Compute the correction

  $$\tilde{\Delta\mathbf{q}} = \tilde{\mathbf{q}}^{n+1} - \tilde{\mathbf{q}}^n \tag{6}$$

  $$\bar{\Delta\mathbf{q}} = \begin{cases} \tilde{\Delta\mathbf{q}} & \text{if } \bar{\mathbf{q}} > \mathbf{0} \\ -\tilde{\Delta\mathbf{q}} & \text{if } \bar{\mathbf{q}} < \mathbf{0} \end{cases} \tag{7}$$

- Step 5.

  Update the dependent variables

  $$\bar{\mathbf{q}}^{n+1} = \bar{\mathbf{q}}^n + \bar{\Delta\mathbf{q}} \tag{8}$$

Steps 1 to 5 are repeated until convergence is attained. The convergence criterias are

$$\frac{RMS\,[NS(\bar{\mathbf{q}}^n)]}{RMS\,[NS(\bar{\mathbf{q}}^1)]} < \epsilon_1 \tag{9}$$

$$\frac{RMS\,[NS((v^1)^n)]}{RMS\,[TERM]} < \epsilon_2 \tag{10}$$

$$TERM = \frac{1}{Re}\frac{\partial}{\partial x^3}(\mu\frac{\partial v^1}{\partial x^3}) \tag{11}$$

$TERM$ is the second normal derivative of v^1 in the x^1-momentum equation and x^1 is the streamvise coordinate direction. Typical values for ϵ_1 range between 10^{-2} and 10^{-1}, and for ϵ_2 between 10^{-4} and 10^{-3}. During the iterative process, the region on which steps 1 to 5 are being employed may be increased or decreased, depending on the solution. When the iteration steps 1 to 5 converge ($\bar{\mathbf{q}}^{n+1} = \bar{\mathbf{q}}^n$), relations (4) and (5) imply that $NS(\bar{\mathbf{q}}) = \mathbf{0}$, ie one obtains a local Navier-Stokes solution. The process is started by defining an initial separation region with an initial solution, which simply is the last upstream boundary layer solution adjusted to the outer inviscid flow.

The interaction with the Euler field is now treated in two ways. For thin separation bubbles equivalent sources are used in the usual way. But if the separation bubble is thick, ie the viscous region is thicker than the first Euler cell at the wall, the viscous solution must be "frozen" in the Euler cells. The matching between the inner (viscous) and the outer (inviscid) solutions takes place at the physical edge of the viscous region, which is resolved also by the Euler grid. The boundary conditions for the Euler calculations are then evaluated using Riemann invariants.

The main advantages of this coupled SOBOL-Euler with local Booster-SOBOL-Euler solver (ESB) compared to a (comparable) Navier-Stokes solver are the following:

1. Accuracy

• The ESB procedure results in a boundary layer solution when this approximation is valid and a local Navier-Stokes solution otherwise, both computed in a mesh with high local resolution.

2. Computational efficiency

• The computational efficiency can be estimated by comparing the Euler solver with a similar Navier-Stokes solver (items **a-c** below), and by comparing the Euler solver with the ESB solver (items **d-e** below). The subject of interest is to estimate the time relations between the different solvers to reach a steady state solution.

a) The extra amount of work for the Navier-Stokes solver is to compute the viscous fluxes. This can be roughly estimated as 3-4 times more operations than the sum of the operations to compute the convective and dissipative fluxes.

b) A severe restriction for the Navier-Stokes solver is the maximum allowable time step limited by the viscous fluxes, cautiously estimated to be 5 times smaller than the Euler time step.

c) The Multi-Grid convergence rate is poor on grids with high aspect ratios (typical for Navier-Stokes). Furthermore, the Navier-Stokes grid accomodates a considerably larger number of grid points as compared to the Euler grid (at least 2 times more). Summing up items **a-c** gives a rough estimate that the Euler steady state is reached 30-40 times faster than the Navier-Stokes steady state.

d) When comparing the ESB solver with the Euler solver it is illuminating to study the convergence history plot in Figure 19. The converged Euler solution is here obtained after 509 work units, while the ESB solution is reached at 716 work units.

e) Looking again at Figure 19 one can note that one ESB coupling consists of 50 Euler time steps plus a SOBOL-Booster evaluation. For this case, the CPU time relation between the SOBOL-Booster calculations (including the interpolations between the Euler and SOBOL meshes) and the 50 Euler time steps is 0.3. The total amount of SOBOL-Booster calculations is 11, ie the total viscous work corresponds to 165 Euler time steps. In other words, the total ESB work is equivalent to $716 + 165 = 881$ Euler work. Comparing item **d** above, the Euler solver is (in this case) $881/509 = 1.73$ times faster than the ESB solver. For a general case with large separation the factor is not likely to be more than 3.

In summary, the ESB solver is estimated to be at least one order of magnitude faster than a comparable Navier-Stokes solver.

• The ESB solver requires considerably less memory storage, since the Booster requires only local storage of the full viscous solution, whereas at non-separated regions the full boundary layer solution is not stored.

• Simpler adaptivity in determining the size of the region where an iterative solution has to be computed.

The method is mostly suitable to situations where there are localized and limited separation bubbles and otherwise larger regions with unseparated flows for which the boundary layer theory is a good approximation. Such flows occur in many practical aeronautical situations, eg wings, wing/body combinations and cascades. Even in case where one has massive separation, the modified boundary layer approach can be used as an efficient solver. The function of the Booster is similar to a preconditioner or a smoother, depending on the context in which it is being used. It is close in character to a Reduced Navier-Stokes (RNS) solver. A more detailed description of the ESB procedure is given by Joona [6].

Computational Results

The described ESB coupling approach has been tested on two-dimensional airfoil configurations and a three-dimensional test wing configuration. The computed set of 2D results involved two different airfoils, the RAE 2822 supercritical airfoil and the classical NACA 0012 airfoil. The computations were performed on three-dimensional straight wing sections, since the computer codes were developed for 3D flows. Periodic boundary conditions were used at the wing root and tip to obtain two-dimensional results. Full 3D calculations were performed on flows around the DLR F5 wing.

RAE 2822

The RAE 2822 wing profile has been studied experimentally by Cook *et al.* [1]. The chosen computational test cases are Case1 and Case10, keeping the

notation from [1], defined in Table 1. The angle of attack was corrected for wall interference as suggested by Firmin and Cook [2].

		Experiment	Computation
Case1	M_∞	0.676	0.676
	α	2.40°	1.98°
	Re	$5.7 \cdot 10^6$	$5.7 \cdot 10^6$
Case10	M_∞	0.750	0.750
	α	3.19°	2.70°
	Re	$6.2 \cdot 10^6$	$6.2 \cdot 10^6$

Table 1: Definition of the flow cases for the RAE 2822 profile. M_∞ is the free stream Mach number, α is the angle of attack and Re is the Reynolds number based on chord length c.

Case1

This is a fully attached flow case. The Euler calculations were performed on a 129x33 O-mesh with 17 span stations. Three Multi-Grid levels were used. SOBOL was solved on the Euler surface mesh (129x17) with 64 points on each boundary layer normal. Transition to turbulence was set at chord station $x/c = 0.11$ as indicated in the experiments. The Cebeci-Smith turbulence model was used. The convergence history is shown in Figure 1. An inviscid solution was first obtained with a full Multi-Grid (FMG) cycle consisting of 50+50+300 time steps. The boundary layer was calculated and the equivalent source distribution was then used to compute the viscous solution with 300 time steps using the saw tooth cycle on the finest Multi-Grid level. In Figure 2 the inviscid and viscous pressure distributions are compared to experimental data. Both computations are close to experiments except near the trailing edge. As expected, the coupled calculation improves the pure inviscid solution. The skin friction coefficient is shown in Figure 3 and the displacement thickness in Figure 4.

Case10

This case has also been studied in a computational workshop described by Holst [4], where a number of Navier-Stokes and inviscid-viscous calculations are presented. It is a "difficult" flow case for which some contributors obtain separation and some do not. The experimental evidence in Cook *et al.* [1] indicates separation to be located somewhere between $x/c > 0.50$ and $x/c < 0.90$. A more precise location is not stated. The same O-mesh was used as in Case1. The inviscid solution was obtained with 50+50+300 time steps and the viscous with 14 couplings times 50 time steps. The Euler convergence history is shown in Figure 5. The messy Euler convergence is probably due to the fact that the Booster is never converged during the first couplings and no reattachment of the boundary layer is obtained. However, the procedure is forced to continue and reattachment is eventually obtained. A thin separation bubble is developed between $x/c = 0.605$ and 0.763. The boundary layer separates again at $x/c = 0.944$. No Booster calculations are tried at this location during the last 4 couplings, since in order to succeed the Booster marching should extend into the wake. The inviscid and viscous pressure distributions are shown in Figure 6. The computed shock is located downstream from the experimental position. The ESB calculations agree with Navier-Stokes calculations that use the Cebeci-Smith turbulence model presented in Holst [4]. The skin friction is shown in Figure 7 and the displacement thickness in Figure 8. δ^* is underestimated when compared to experiments. From the velocity profiles in Figures 9-12 one can see that also the boundary layer thickness is underestimated. The separation bubble is very thin and the matching of the boundary layer to the inviscid flow is quite sharp.

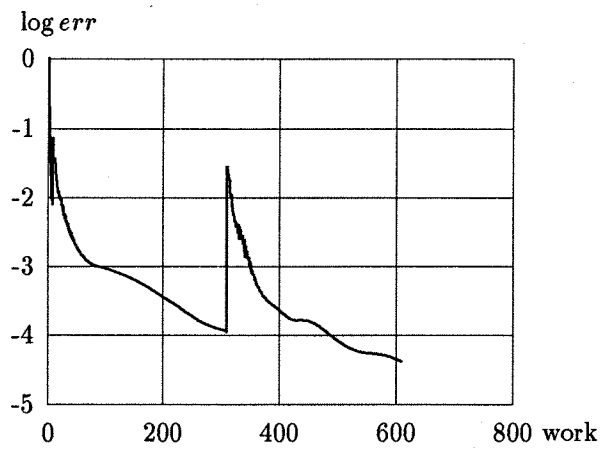

Figure 1. Convergence history for RAE 2822 Case1. *err* is the rms-error of the Euler continuity equation residues.

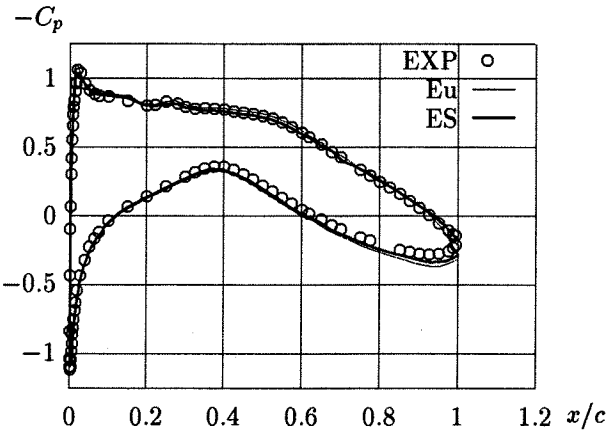

Figure 2. Pressure coefficient C_p for RAE 2822 Case1. EXP are experimental data from Cook *et al.* [1]. Eu is the inviscid Euler solution and ES is the coupled Euler/boundary layer calculation.

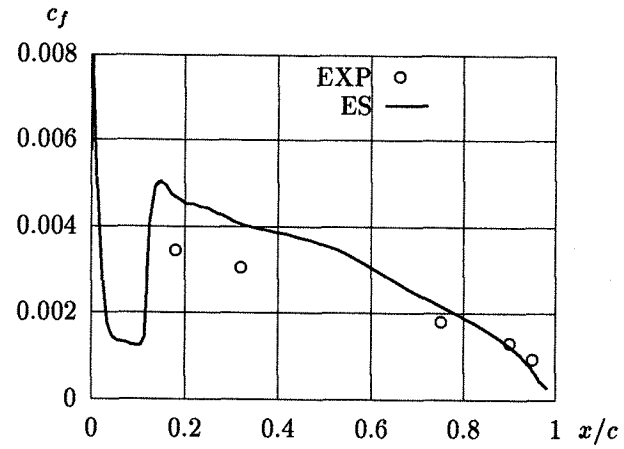

Figure 3. Friction coefficient c_f on the upper side of the wing, RAE 2822 Case1. EXP are experimental data from Cook *et al.* (1) and ES is a coupled Euler/boundary layer calculation.

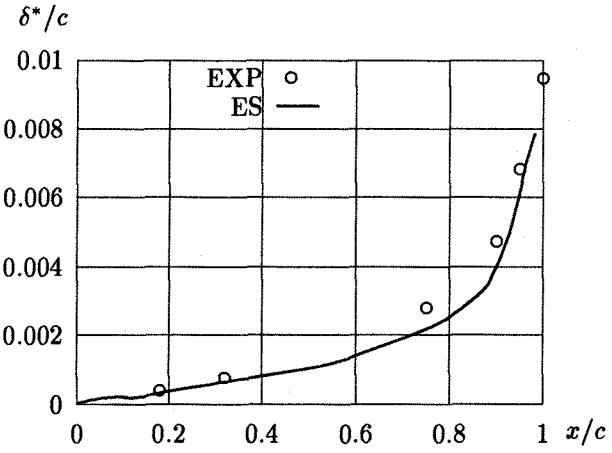

Figure 4. Displacement thickness δ^*/c on the upper side of the wing, RAE 2822 Case1. EXP are experimental data from Cook *et al.* (1) and ES is a coupled Euler/boundary layer calculation.

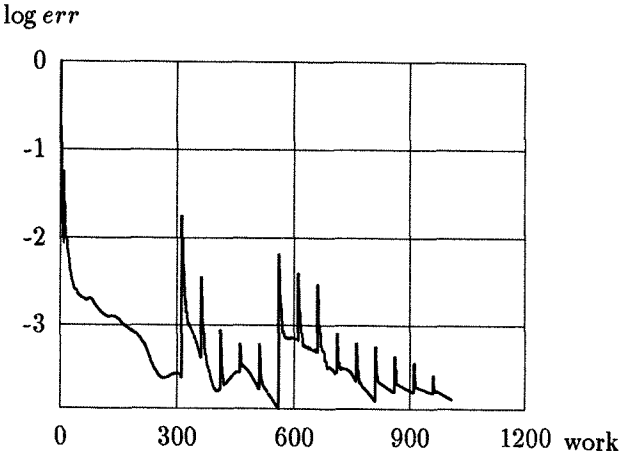

Figure 5. Convergence history for RAE 2822 Case10. *err* is the rms-error of the Euler continuity equation residues.

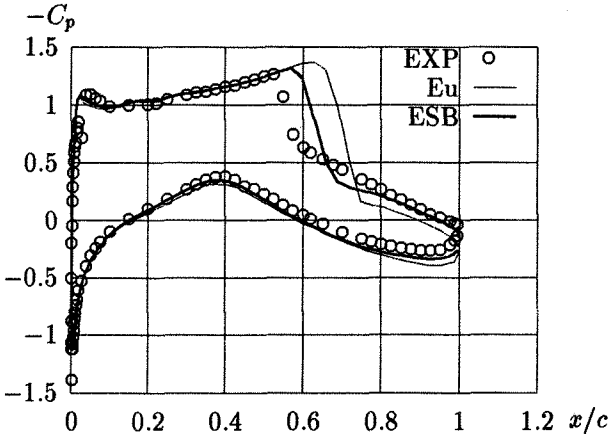

Figure 6. Pressure coefficient C_p for RAE 2822 Case10. EXP are experimental data for Case10 in Cook *et al.* (1).

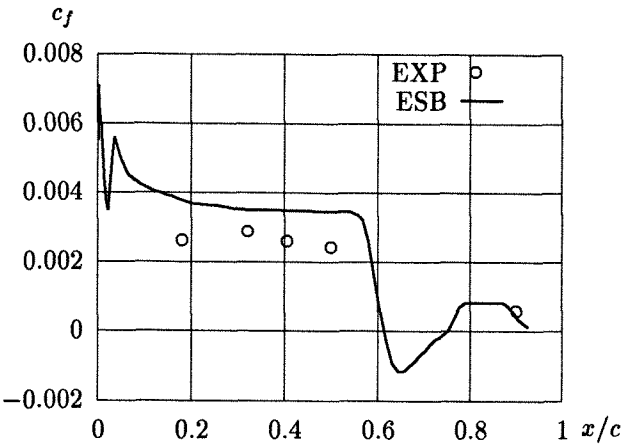

Figure 7. Friction coefficient, c_f, on the upper side of the wing, RAE 2822 Case10. EXP are experimental data from Cook *et al.* (1).

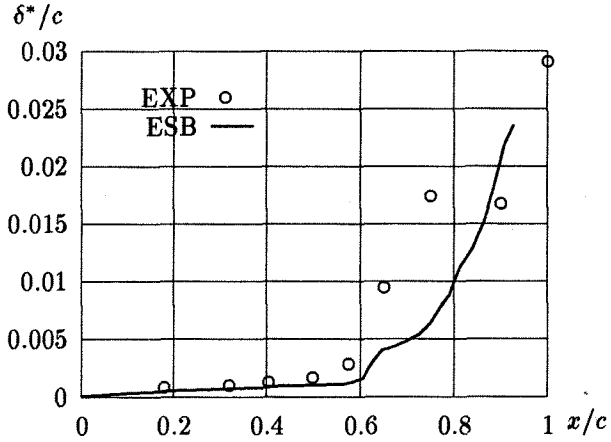

Figure 8. Displacement thickness δ^*/c on the upper side of the wing, RAE 2822 Case10. EXP are experimental data from Cook *et al.* (1).

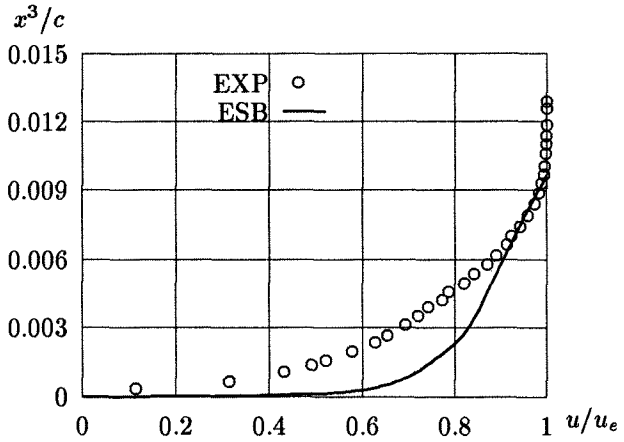

Figure 9. Velocity profiles on the upper side of the wing, RAE 2822 Case10. EXP are experimental data from Cook *et al.* [1] located at $x/c = 0.574$. The ESB calculation is located at $x/c = 0.584$.

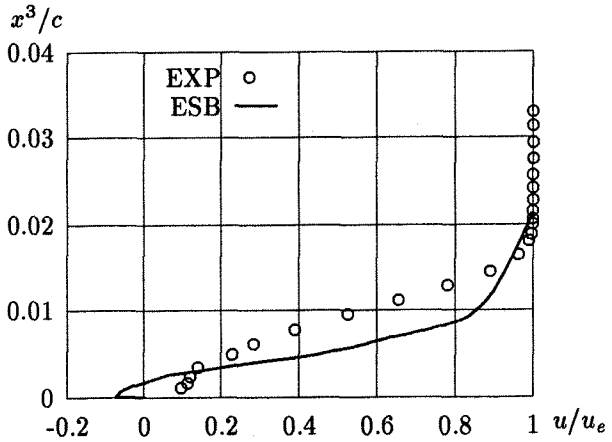

Figure 10. Velocity profiles on the upper side of the wing, RAE 2822 Case10. EXP are experimental data from Cook *et al.* [1] located at $x/c = 0.650$. The ESB calculation is located at $x/c = 0.644$.

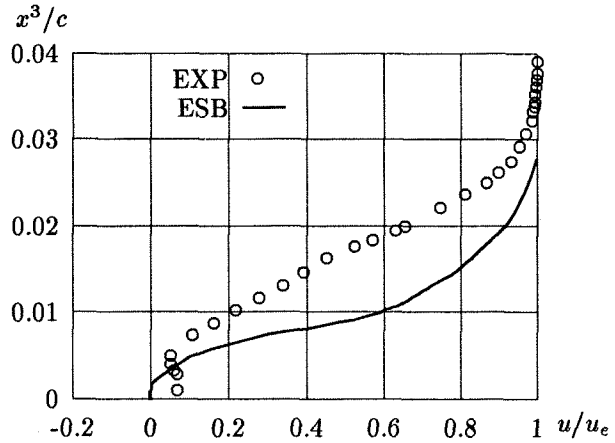

Figure 11. Velocity profiles on the upper side of the wing, RAE 2822 Case10. EXP are experimental data from Cook *et al.* [1] located at $x/c = 0.750$. The ESB calculation is located at $x/c = 0.736$.

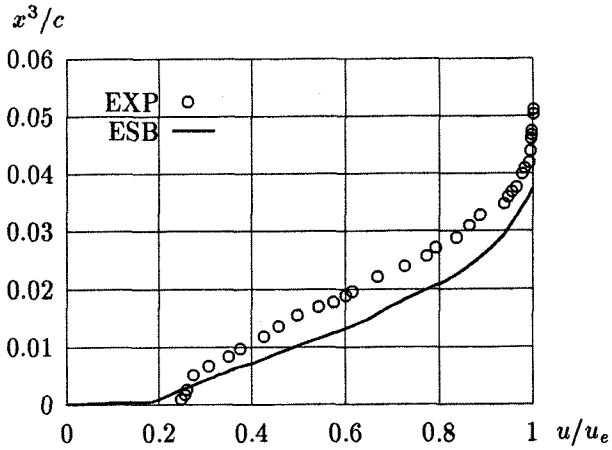

Figure 12. Velocity profiles on the upper side of the wing, RAE 2822 Case10. EXP are experimental data from Cook *et al.* [1] located at $x/c = 0.900$. The ESB calculation is located at $x/c = 0.904$.

NACA 0012

Two flow cases were studied for the NACA 0012 profile. They are defined in Table 2. The experimental data and the α-corrections due to wind tunnel wall interference are given by Harris [3]. The Euler calculations were performed on a 129×33 O-mesh with 17 span stations. Three Multi-Grid levels were used to speed up the convergence. SOBOL used the same surface mesh, ie 129×17 nodes, and 64 nodes in the surface normal direction. The Cebeci-Smith turbulence model was used in all calculations. Transition was set at $x/c = 0.053$ on the upper side, and at $x/c = 0.375$ and $x/c = 0.309$ for Case A2 and A3 respectively on the lower side.

		Experiment	Computation
Case A2	M_∞	0.55	0.55
	α	9.86°	8.34°
	Re	$9 \cdot 10^6$	$9.0 \cdot 10^6$
Case A3	M_∞	0.799	0.799
	α	2.86°	2.26°
	Re	$9 \cdot 10^6$	$9.2 \cdot 10^6$

Table 2: Definition of the flow cases for the NACA 0012 airfoil. M_∞ is the free stream Mach number, α is the angle of attack and Re is the Reynolds number based on chord length c.

Case A2

This is a very interesting flow case. The angle of attack is about one degree below the maximum lift value. In Figure 13 the pressure distributions from an ordinary Euler-boundary layer coupling and from an ESB coupling are compared. The basic Euler-boundary layer coupling indicates separation at $x/c = 0.181$, ie at the foot of the shock resulting in extrapolated sources in a region covering approximately 80 % of the upper surface. When the Navier-Stokes Booster is activated an initial separation region is obtained. As the coupling iterations proceed the separated region becomes smaller until it vanishes. The shock has moved upstream a distance $x/c = 0.03$ towards the experimental shock. This case has also been tested in Holst [4] with indications of a small separation bubble immediately after the shock. The Booster results were obtained by 50+50+200 inviscid time steps and 10×50 viscous time steps.

By raising α to 8.5° a larger separation region is obtained. A detail at the trailing edge is shown in Figure 14. The Booster procedure should extend into the wake but this was not the case here. This case demonstrates that the method is capable to predict flows with larger separated regions.

Case A3

This is a case with a large region of separation from $x/c = 0.57$ to 0.83. The computations started also here with an inviscid solution of 50+50+200 time steps followed by a viscous solution of 10×50 time steps. The Euler convergence is shown in Figure 15.

The C_p-distributions from an Euler-SOBOL coupling and from an ESB coupling are shown in Figure 16. Once again the Boostered calculation moved the shock closer to the experimental location. This case is also studied in Holst [4]. A large scatter in the presented results indicates that the chosen turbulence model has an important influence in the final results. The ESB calculations agree with Navier-Stokes calculations that use the Cebeci-Smith turbulence model presented in Holst [4]. The skin friction coefficient is shown in Figure 17. The flow separates just upstream of the shock, reattaches at $x/c = 0.83$ and separates once again at $x/c = 0.956$.

An attempt to predict a larger separation is shown in Figure 18. Here $M_\infty = 0.7$ and $\alpha = 6°$. The solution is converged and stable. To get higher resolution mesh refinement was introduced at the trailing edge region. This resulted in an unstable solution which can be explained by the fact that the real physical flow is probably time dependent due to vortex shedding at this high angle of attack.

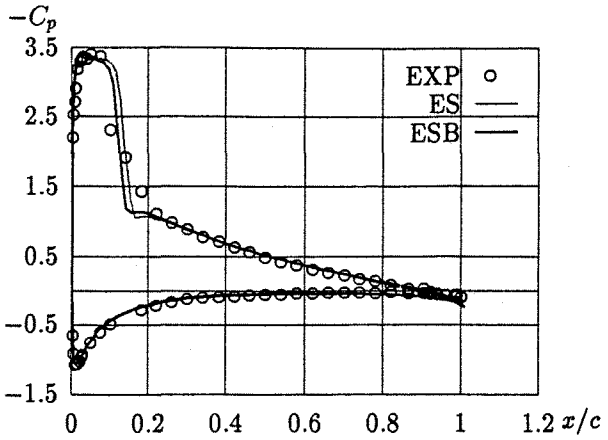

Figure 13. Pressure coefficient C_p for NACA 0012 Case A2. EXP are experimental data from Harris [3]. ES is a coupled Euler/boundary layer calculation.

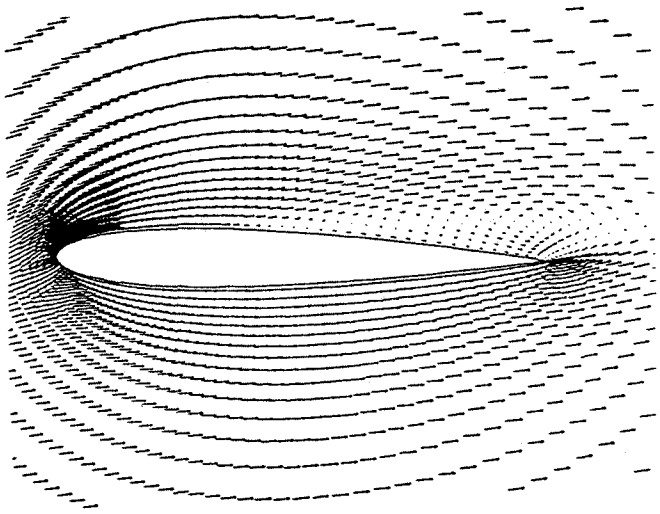

Figure 14. Detail of the NACA 0012 trailing edge at $M_\infty = 0.55$ and $\alpha = 8.5°$. Notice the shock at a chord station of $x/c \approx 0.2$.

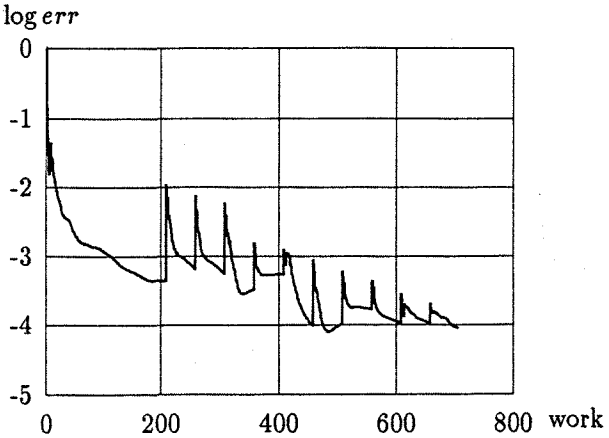

Figure 15. Convergence history for NACA 0012 Case A3. *err* is the rms-error of the Euler continuity equation residues.

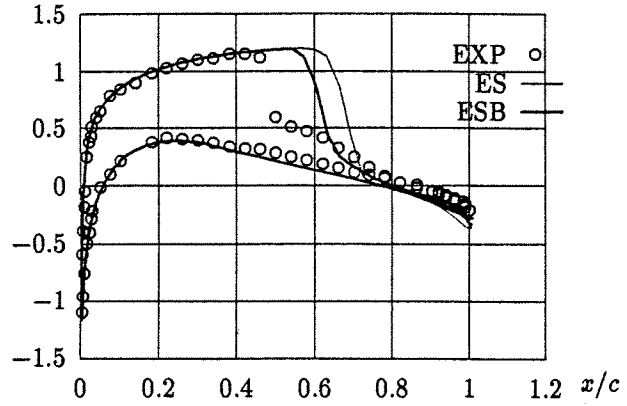

Figure 16. C_p-distributions for the NACA 0012 airfoil Case A3. EXP are experimental data from Harris [3]. ES is a coupled Euler/SOBOL calculation.

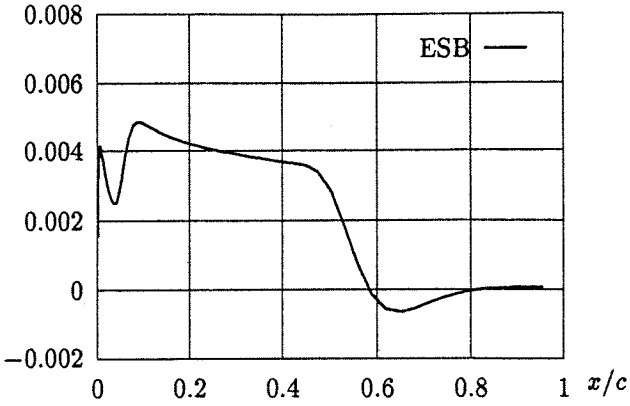

Figure 17. Friction coefficient on the upper side of the NACA 0012 airfoil, Case A3.

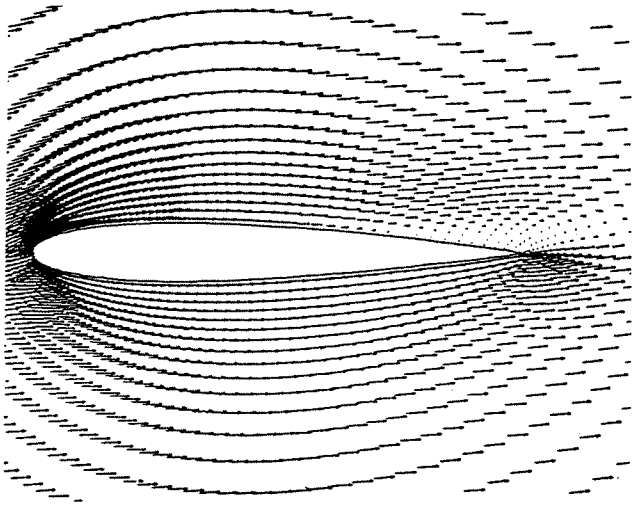

Figure 18. Detail of the NACA 0012 trailing edge at $M_\infty = 0.7$ and $\alpha = 6.0°$.

DLR F5 Wing

In Kordulla [7] the proceedings of a workshop on three-dimensional Navier-Stokes calculations around the DLR F5 wing are reported. The wing geometry was designed as a 20° swept wing with an aspect ratio of 9. The main portion of the wing consists of sections similar to a NACA 6-Series airfoil designed for shock free flow at $M_\infty = 0.78$. The root section is formed by a gradual change to a NACA 0036 airfoil with a large fairing region simulating a wing-body junction. A more detailed description of the wing is found in Sobieczky [12]. The free air test case computed here, denoted B2 in Kordulla [7], is defined in Table 3. The Reynolds number, based on root chord, is $3.6 \cdot 10^6$.

Initially, transition was specified using the curve fit given by Sobieczky [12]. This analytical model for the transition line is derived from wind tunnel visualizations. The flow is fully turbulent from the wing root out to $y/y_{span} = 0.07$. In the remaining part of the wing transition occurs mainly in the region from $x/C = 0.40$ to $x/C = 0.60$. Here C denotes the local chord. It was impossible to simulate this on the upper side, since the laminar boundary layer separated far upstream of the specified transition line. Hence it was decided to set transition at $x/C = 0.05$ on the upper side. This makes it questionable to compare the results with the Navier-Stokes data in Kordulla [7]. However, another workshop on this wing has been carried out with wind tunnel simulations using the same transition specification as here. That workshop data are presented by Schwamborn and Rung [11]. The Euler calculations were performed on a 129×33×33 OO-mesh using 4 Multi-Grid levels. The boundary layer was calculated on the same surface mesh 129×33 with 64 points in the normal direction. No boundary layer calculations could be performed at the wing root section due to the geometry there. The tip vortex resulting from the Euler calculations made it also impossible to calculate the boundary layer at the wing tip. The region for the boundary layer calculations is from $y/y_{span} = 0.015$ to $y/y_{span} = 0.98$. Free boundary conditions were used at the lateral boundaries and the equivalent sources were extrapolated to the remaining sections of the wing. Once again, the Cebeci-Smith turbulence model was used in all calculations.

		Definition	Computation
Case B2	M_∞	0.82	0.82
	α	2°	2°
	Re/meter	10^7	$9.9 \cdot 10^6$

Table 3: Definition of the computed case for the DLR F5 wing. M_∞ is the free stream Mach number, α is the angle of attack and Re is the Reynolds number.

The inviscid solution was obtained with an FMG consisting of 50+50+50+200 time steps and the viscous coupling used 10 × 50 time steps. The Euler convergence is shown in Figure 19. Figures 20 to 22 show the C_p-distributions at three different span stations. The experimental data are obtained from Kordulla [7]. They are wind tunnel data, while the computed case is in free air. The experimental data are shown here as a reference. The calculated results are in good agreement with the Navier-Stokes results presented in Kordulla [7], (with reservation to the transition line definitions...). The most evident differencies are:

- There is a plateau in the experimental C_p-values on the wing upper side just upstream of the shock. This is interpreted as a laminar separation bubble. All Navier-Stokes contributors except one predict a suction peak in the plateau region at Sections 4 and 6. In the present calculation the flow is turbulent here. A separation bubble begins just upstream of the shock for all three sections.
- The computed shock strengths are weaker at all sections. The shock locations at Sections 6 and 8 are approximately a distance $x/C = 0.05$ upstream of the predicted locations in Kordulla [7].
- In the present calculation there is some wiggles in the C_p-curves at the trailing edge. No such behaviour is observed in Kordulla [7]. The wiggles are probably caused by the Euler mesh, since it is rather coarse at this region.

Separation occurs between $x/C = 0.684$ and $x/C = 0.767$ at $y/y_{span} = 0.191$, between $x/C = 0.661$ and $x/C = 0.748$ at $y/y_{span} = 0.515$, and between $x/C = 0.613$ and $x/C = 0.706$ at $y/y_{span} = 0.814$. The flow reattaches and separates again at the trailing edge. On the lower side separation occurs at the inner aft portion of the wing, hence no Booster calculations are tried here.

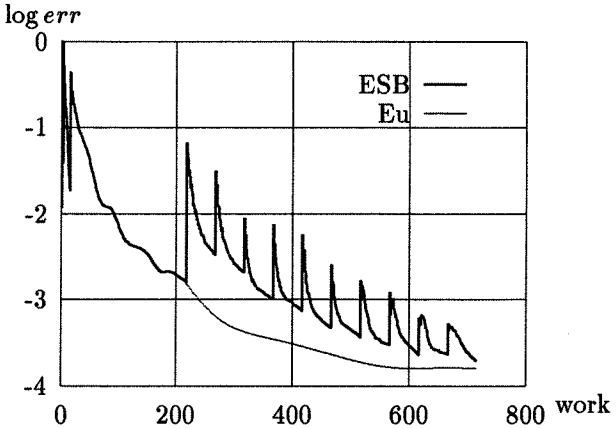

Figure 19. Convergence history for Case B2. *err* is the rms-error of the Euler continuity equation residues. The ESB procedure consists of 216 inviscid Euler work + 10 × 50 viscous Euler work. Eu is a purely inviscid Euler computation of 716 work.

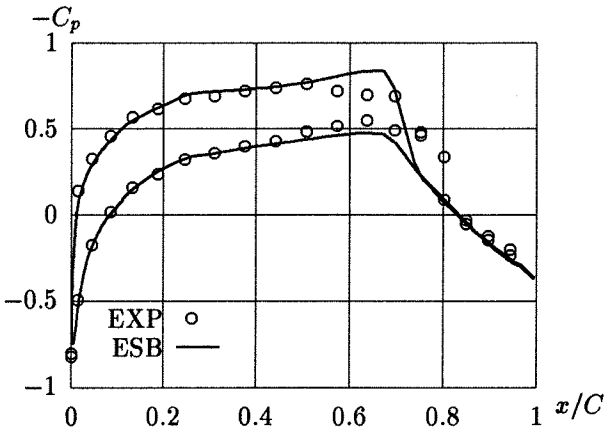

Figure 20. Pressure coefficient C_p for the DLR F5 wing at section 4. EXP are experimental data from Kordulla [6] at $y/y_{span} = 0.205$. The ESB results are at $y/y_{span} = 0.212$. C denotes the local chord length.

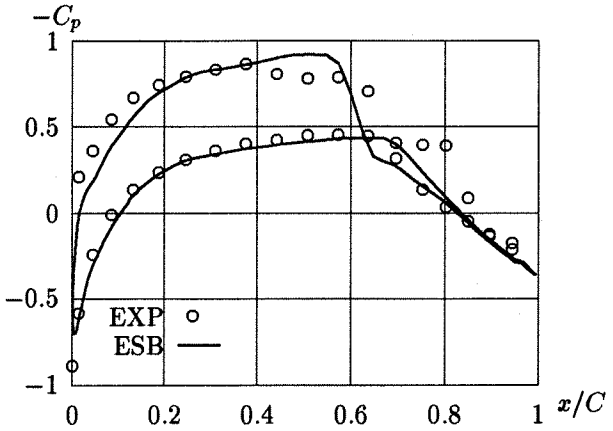

Figure 21. Pressure coefficient C_p for the DLR F5 wing at section 8. EXP are experimental data from Kordulla [6] at $y/y_{span} = 0.8$. The ESB results are at $y/y_{span} = 0.796$. C denotes the local chord length.

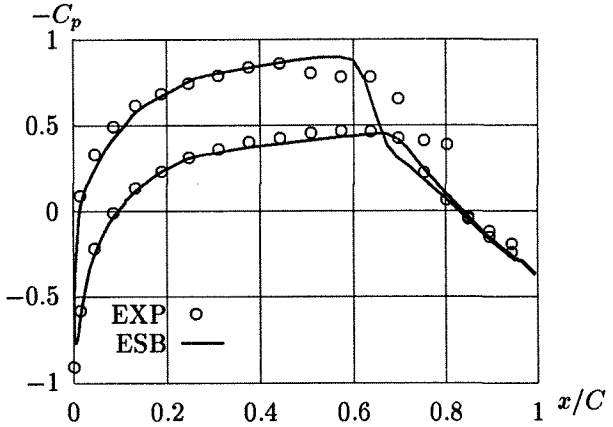

Figure 22. Pressure coefficient C_p for the DLR F5 wing at section 6. EXP are experimental data from Kordulla [6] at $y/y_{span} = 0.492$. The ESB results are at $y/y_{span} = 0.491$. C denotes the local chord length.

Conclusions

Separated flows can be predicted with a direct iteration method for interactive Euler-boundary layer calculations. The tool for this is to include a correction in the boundary layer operator so that in effect one solves the Navier-Stokes problem. The method works for both two- and three-dimensional transonic flows around wing configurations. The computed test cases imply that a better accuracy can be gained if the method is extended to include wake flows.

The computational effort saved with the direct inviscid-viscous coupling method is considerable (at least an order of magnitude). Together with the ability of predicting separation makes this method to be an important tool for aerodynamic design purposes.

Further investigations must be performed with respect to the influence of the presumed transition line regions. The sensitivity to transitional flows and the effects of using different turbulence models must be investigated. These questions are equally open for the coupled method presented here as for a full Navier-Stokes solver.

References

1. Cook P.H. , McDonald M.A. and Firmin M.C.P. *Aerofoil RAE 2822 - Pressure distributions, and boundary layer and wake measurements.* AGARD-AR-138, 1979.

2. Firmin M.C.P. and Cook P.H. *Disturbances from ventilated tunnel walls in aerofoil testing.* AGARD-CP-348, 1983.

3. Harris C.D. *Two-Dimensional Aerodynamic Characteristics of the NACA 0012 Airfoil in the Langley 8-Foot Transonic Pressure Tunnel.* NASA TM 81927, 1981.

4. Holst T.L. *Viscous Transonic Airfoil Workshop Compendium of Results.* AIAA Paper 87-1460, 1987.

5. Jameson A. *Numerical solution of the Euler equation for compressible inviscid fluids.* Proc of the INRIA Workshop on Numerical Methods for the Euler Equations of Fluid Dynamics, Rocquenfort, 1983, edited by F. Angrand et al., SIAM, pp 199-245.

6. Joona H. *An Inviscid-Viscous Coupling Method for 3D Transonic Separated Flows.* TRITA-MEK-94-08, ISSN 0348-467X, 1994.

7. Kordulla W. (editor). *Numerical Simulation of the Transonic DFVLR-F5 Wing Experiment.* Notes on Numerical Fluid Mechanics, Volume 22, 1988, Vieweg.

8. Lighthill M.J. *On displacement thickness.* JFM 4, 1958, pp 383-392.

9. Monnoyer F. *The effect of surface curvature on three-dimensional, laminar boundary layers.* Doctoral Thesis Université libre de Bruxelles, 1985.

10. Monnoyer F. *Calculation of three-dimensional attached viscous flow on general configurations using second-order boundary layer theory.* ZFW 14, 1990, pp 95-108.

11. Schwamborn D. and Rung T. *The DLR-F5 Wing Test Case.* In Notes on Numerical Fluid Mechanics, Volume 42, 1993, Vieweg.

12. Sobieczky H. *DLR-F5 Test Wing Configuration for Computational and Experimental Aerodynamics.* DLR IB 221 - 87 A 01, 1987. Reprint with an Update 1991.

13. Van Dyke M. *Perturbation Methods in Fluid Mechanics.* Academic Press, New-York, 1964.

14. Whitfield D.L. , Swafford T.W. and Jacocks J.L. *Calculation of Turbulent Boundary Layers with Separation and Viscous-Inviscid Interaction.* AIAA Journal, Volume 19, Number 10, 1981, pp 1315-1322.